Supplementary Information for A Computational Dieke Design Map for Near-Infrared Optical Absorption in Transition Metal-Substituted Yttria-Stabilized Zirconia

Shunshun Liu,[1,*] David R. Clarke,[2,†] and Prasanna V. Balachandran[1,‡]

[1]*Department of Materials Science and Engineering, University of Virginia, Charlottesville, VA 22903, USA.*

[2]*Harvard John A. Paulson School of Engineering and Applied Sciences, Harvard University, Cambridge, MA, USA*

(Dated: February 19, 2026)

* ejf5wk@virginia.edu

† clarke@seas.harvard.edu

‡ pvb5e@virginia.edu

S1. OPTICAL PROPERTIES OF ALL CONFIGURATIONS

S1.1. Ti^{4+}

(a) Real part of the dielectric function (ϵ_1)

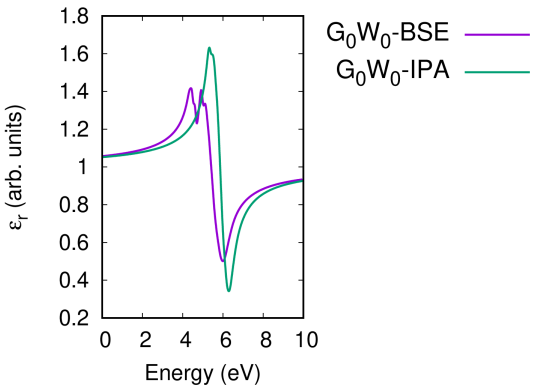

(b) Imaginary part of the dielectric function (ϵ_2)

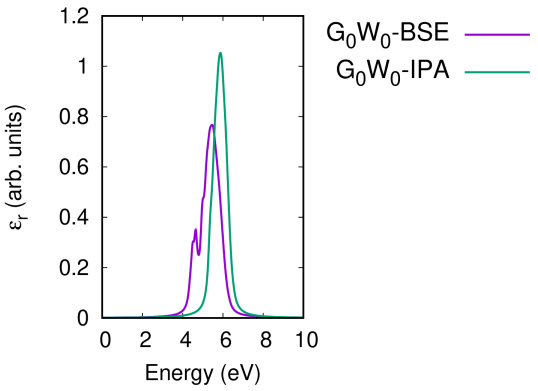

(c) Calculated optical absorption spectrum

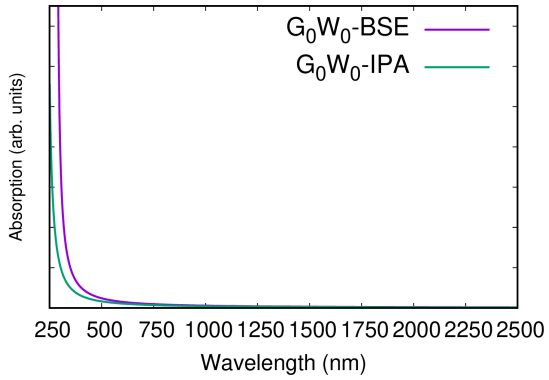

Figure S1: The relative dielectric function ϵ_r(E) is defined as ϵ_r(E) = ϵ_1(E) + $i\epsilon_2$(E), where ϵ_1 and ϵ_2 are the real and imaginary parts of the dielectric function, respectively, and E is the photon energy (eV) related to wavelength λ (nm) through E = $\frac{1239.8}{\lambda}$. In (a) and (b) we show the ϵ_1(E) and ϵ_2(E) as a function of photon energy for Ti^{4+}-substituted t-YSZ configurations, respectively. The optical absorption spectrum is shown in (c). The color of the curve indicates different approximation level, where purple curve stands for G_0W_0-BSE and the green curve indicates the G_0W_0-IPA.

S1.2. V^{3+}

(a) Real part of the dielectric function (ϵ_1)

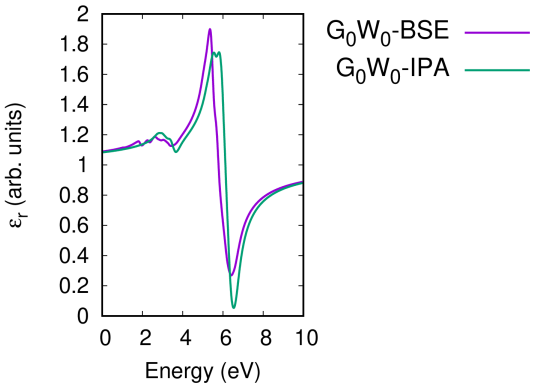

(b) Imaginary part of the dielectric function (ϵ_2)

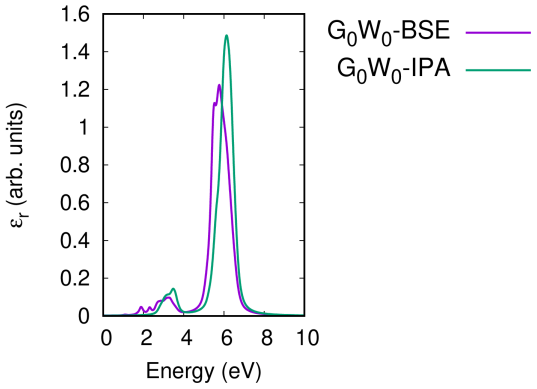

(c) Calculated optical absorption spectrum

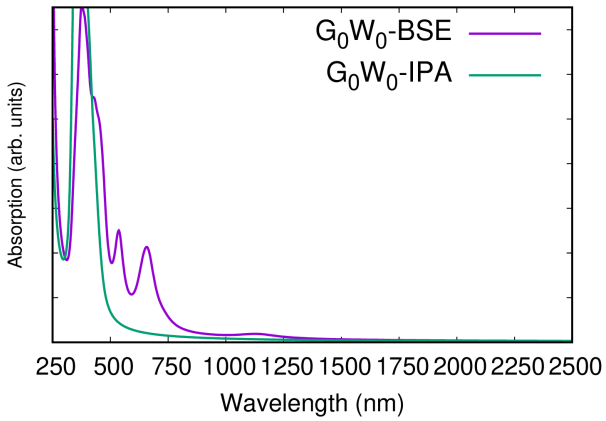

Figure S2: The relative dielectric function $\epsilon_r(\mathrm{E})$ is defined as $\epsilon_r(\mathrm{E}) = \epsilon_1(\mathrm{E}) + i\epsilon_2(\mathrm{E})$, where ϵ_1 and ϵ_2 are the real and imaginary parts of the dielectric function, respectively, and E is the photon energy (eV) related to wavelength λ (nm) through $\mathrm{E} = \frac{1239.8}{\lambda}$. In (a) and (b) we show the $\epsilon_1(\mathrm{E})$ and $\epsilon_2(\mathrm{E})$ as a function of photon energy for V^{3+}-substituted t-YSZ configurations, respectively. The optical absorption spectrum is shown in (c). The color of the curve indicates different approximation level, where purple curve stands for G_0W_0-BSE and the green curve indicates the G_0W_0-IPA.

S1.3. Cr^{3+}

(a) Real part of the dielectric function (ϵ_1)

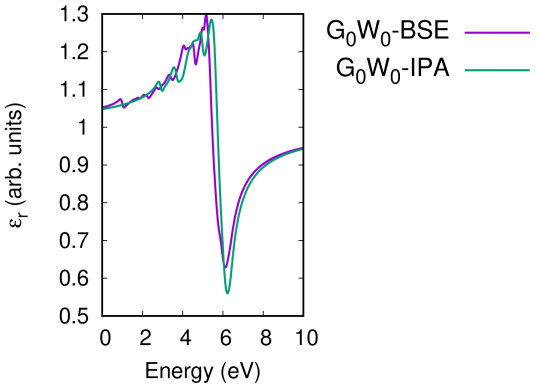

(b) Imaginary part of the dielectric function (ϵ_2)

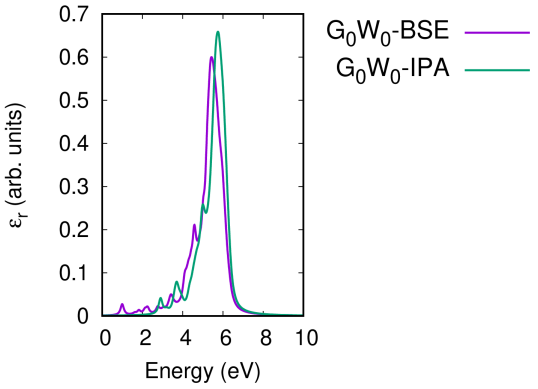

(c) Calculated optical absorption spectrum

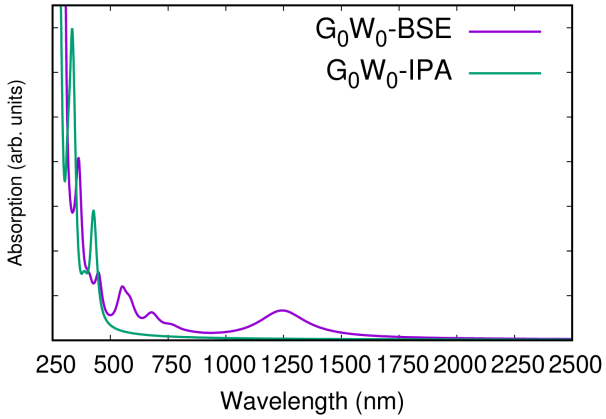

Figure S3: The relative dielectric function $\epsilon_r(\mathrm{E})$ is defined as $\epsilon_r(\mathrm{E}) = \epsilon_1(\mathrm{E}) + i\epsilon_2(\mathrm{E})$, where ϵ_1 and ϵ_2 are the real and imaginary parts of the dielectric function, respectively, and E is the photon energy (eV) related to wavelength λ (nm) through $\mathrm{E} = \frac{1239.8}{\lambda}$. In (a) and (b) we show the $\epsilon_1(\mathrm{E})$ and $\epsilon_2(\mathrm{E})$ as a function of photon energy for Cr^{3+}-substituted t-YSZ configurations, respectively. The optical absorption spectrum is shown in (c). The color of the curve indicates different approximation level, where purple curve stands for G_0W_0-BSE and the green curve indicates the G_0W_0-IPA.

S1.4. Cr^{6+}

(a) Real part of the dielectric function (ϵ_1)

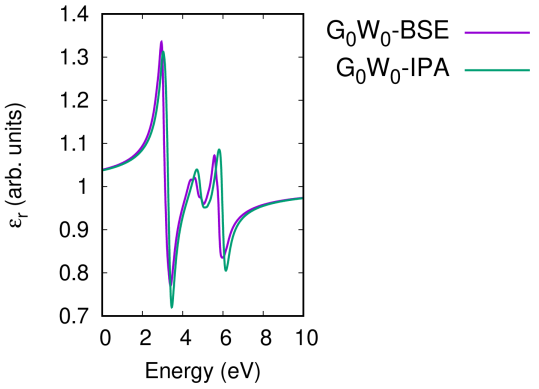

(b) Imaginary part of the dielectric function (ϵ_2)

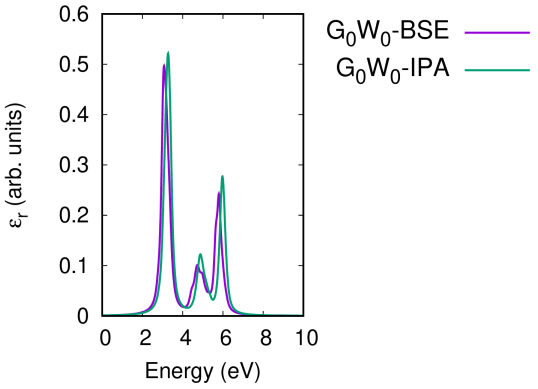

(c) Calculated optical absorption spectrum

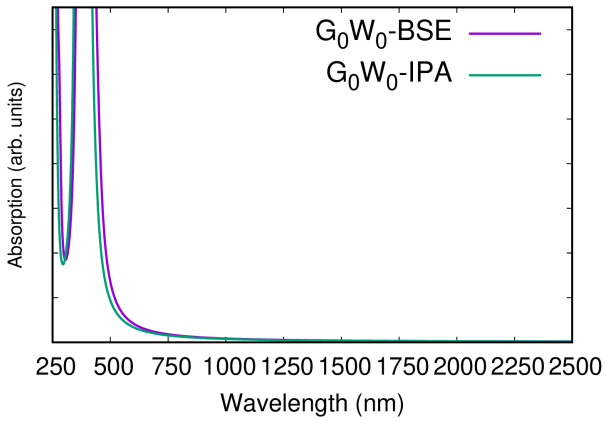

Figure S4: The relative dielectric function $\epsilon_r(\mathrm{E})$ is defined as $\epsilon_r(\mathrm{E}) = \epsilon_1(\mathrm{E}) + i\epsilon_2(\mathrm{E})$, where ϵ_1 and ϵ_2 are the real and imaginary parts of the dielectric function, respectively, and E is the photon energy (eV) related to wavelength λ (nm) through $\mathrm{E} = \frac{1239.8}{\lambda}$. In (a) and (b) we show the $\epsilon_1(\mathrm{E})$ and $\epsilon_2(\mathrm{E})$ as a function of photon energy for Cr^{6+}-substituted t-YSZ configurations, respectively. The optical absorption spectrum is shown in (c). The color of the curve indicates different approximation level, where purple curve stands for G_0W_0-BSE and the green curve indicates the G_0W_0-IPA.

S1.5. Mn^{2+}

(a) Real part of the dielectric function (ϵ_1)

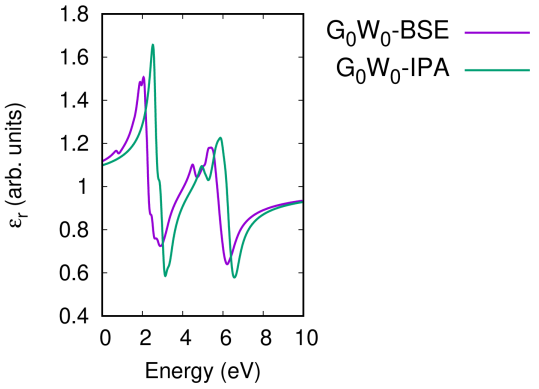

(b) Imaginary part of the dielectric function (ϵ_2)

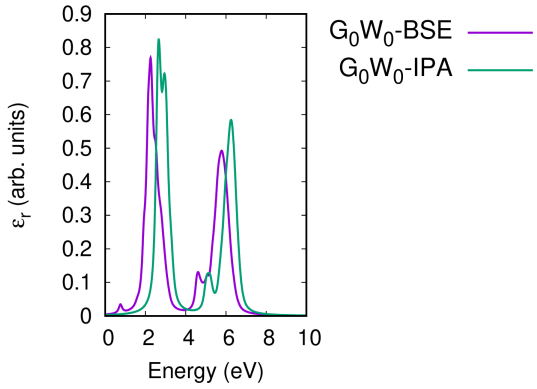

(c) Calculated optical absorption spectrum

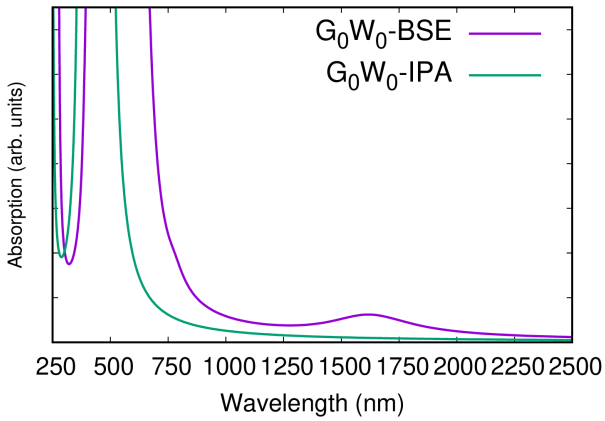

Figure S5: The relative dielectric function $\epsilon_r(\mathrm{E})$ is defined as $\epsilon_r(\mathrm{E}) = \epsilon_1(\mathrm{E}) + i\epsilon_2(\mathrm{E})$, where ϵ_1 and ϵ_2 are the real and imaginary parts of the dielectric function, respectively, and E is the photon energy (eV) related to wavelength λ (nm) through $\mathrm{E} = \frac{1239.8}{\lambda}$. In (a) and (b) we show the $\epsilon_1(\mathrm{E})$ and $\epsilon_2(\mathrm{E})$ as a function of photon energy for Mn^{2+}-substituted t-YSZ configurations, respectively. The optical absorption spectrum is shown in (c). The color of the curve indicates different approximation level, where purple curve stands for G_0W_0-BSE and the green curve indicates the G_0W_0-IPA.

S1.6. Mn^{3+}

(a) Real part of the dielectric function (ϵ_1)

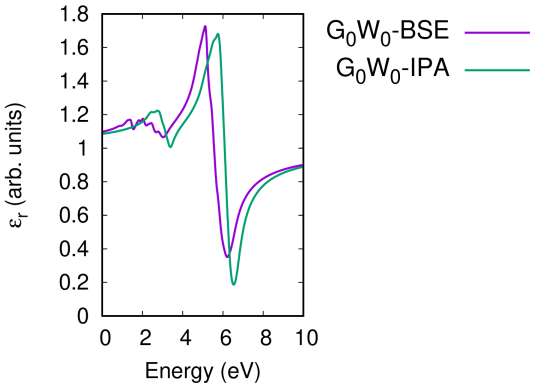

(b) Imaginary part of the dielectric function (ϵ_2)

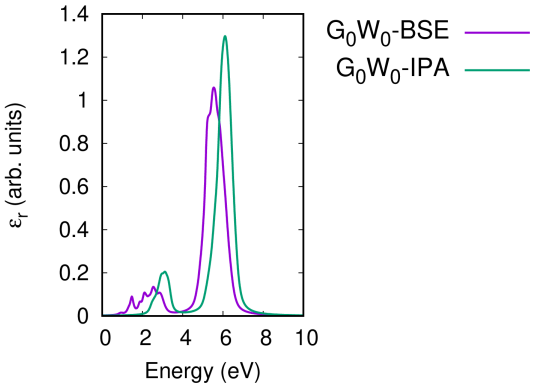

(c) Calculated optical absorption spectrum

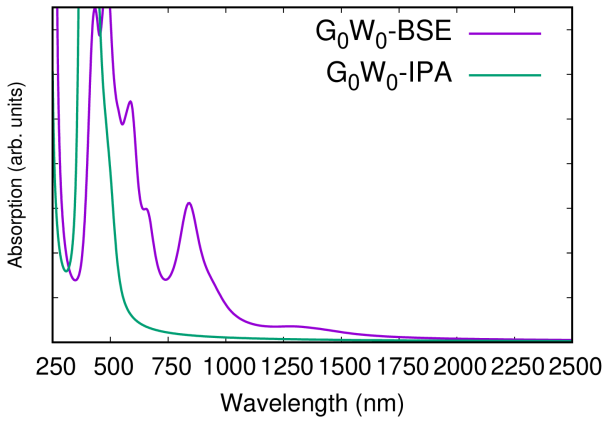

Figure S6: The relative dielectric function $\epsilon_r(\mathrm{E})$ is defined as $\epsilon_r(\mathrm{E}) = \epsilon_1(\mathrm{E}) + i\epsilon_2(\mathrm{E})$, where ϵ_1 and ϵ_2 are the real and imaginary parts of the dielectric function, respectively, and E is the photon energy (eV) related to wavelength λ (nm) through $\mathrm{E} = \frac{1239.8}{\lambda}$. In (a) and (b) we show the $\epsilon_1(\mathrm{E})$ and $\epsilon_2(\mathrm{E})$ as a function of photon energy for Mn^{3+}-substituted t-YSZ configurations, respectively. The optical absorption spectrum is shown in (c). The color of the curve indicates different approximation level, where purple curve stands for G_0W_0-BSE and the green curve indicates the G_0W_0-IPA.

S1.7. Mn^{4+}

(a) Real part of the dielectric function (ϵ_1)

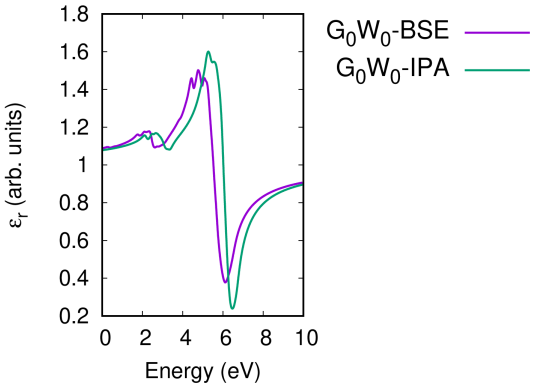

(b) Imaginary part of the dielectric function (ϵ_2)

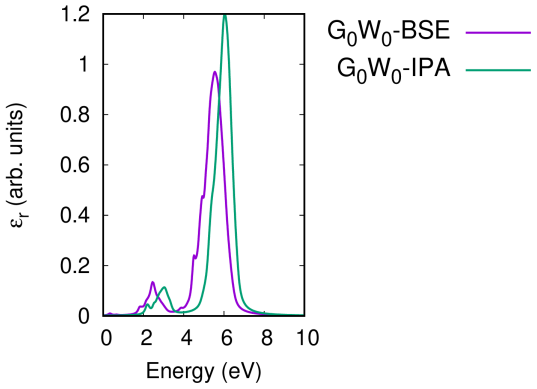

(c) Calculated optical absorption spectrum

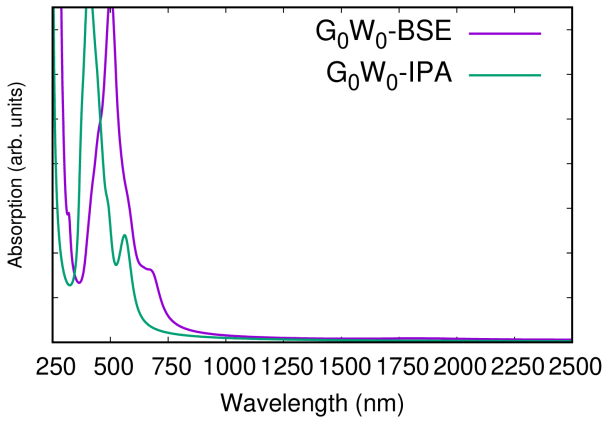

Figure S7: The relative dielectric function ϵ_r(E) is defined as ϵ_r(E) = ϵ_1(E) + $i\epsilon_2$(E), where ϵ_1 and ϵ_2 are the real and imaginary parts of the dielectric function, respectively, and E is the photon energy (eV) related to wavelength λ (nm) through E = $\frac{1239.8}{\lambda}$. In (a) and (b) we show the ϵ_1(E) and ϵ_2(E) as a function of photon energy for Mn^{4+}-substituted t-YSZ configurations, respectively. The optical absorption spectrum is shown in (c). The color of the curve indicates different approximation level, where purple curve stands for G_0W_0-BSE and the green curve indicates the G_0W_0-IPA.

S1.8. Fe^{3+}

(a) Real part of the dielectric function (ϵ_1)

(b) Imaginary part of the dielectric function (ϵ_2)

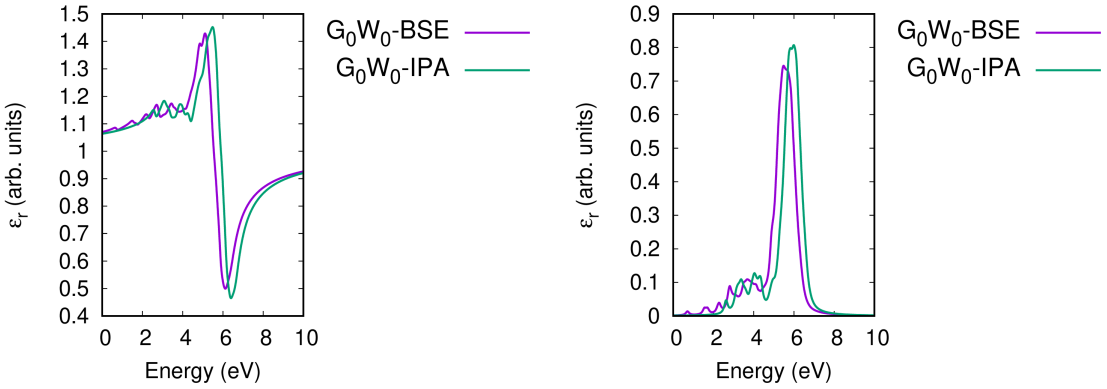

(c) Calculated optical absorption spectrum

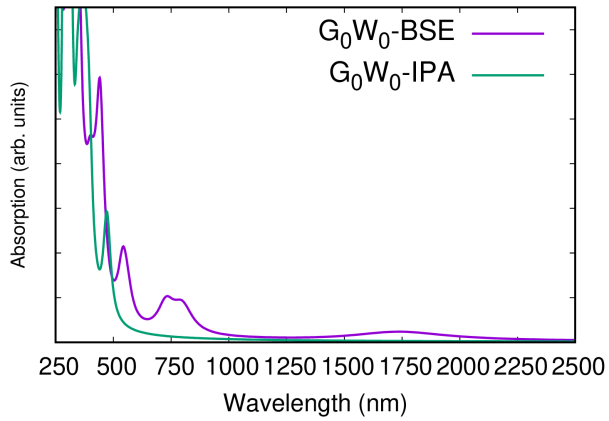

Figure S8: The relative dielectric function $\epsilon_r(\mathrm{E})$ is defined as $\epsilon_r(\mathrm{E}) = \epsilon_1(\mathrm{E}) + i\epsilon_2(\mathrm{E})$, where ϵ_1 and ϵ_2 are the real and imaginary parts of the dielectric function, respectively, and E is the photon energy (eV) related to wavelength λ (nm) through $\mathrm{E} = \frac{1239.8}{\lambda}$. In (a) and (b) we show the $\epsilon_1(\mathrm{E})$ and $\epsilon_2(\mathrm{E})$ as a function of photon energy for Fe^{3+}-substituted t-YSZ configurations, respectively. The optical absorption spectrum is shown in (c). The color of the curve indicates different approximation level, where purple curve stands for G_0W_0-BSE and the green curve indicates the G_0W_0-IPA.

S1.9. Co^{3+}

(a) Real part of the dielectric function (ϵ_1)

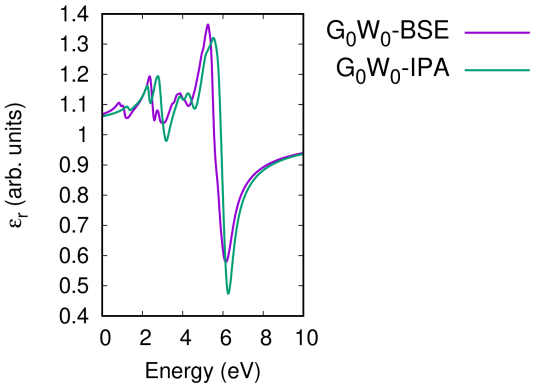

(b) Imaginary part of the dielectric function (ϵ_2)

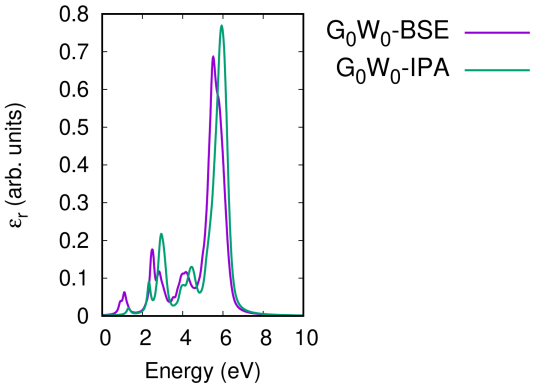

(c) Calculated optical absorption spectrum

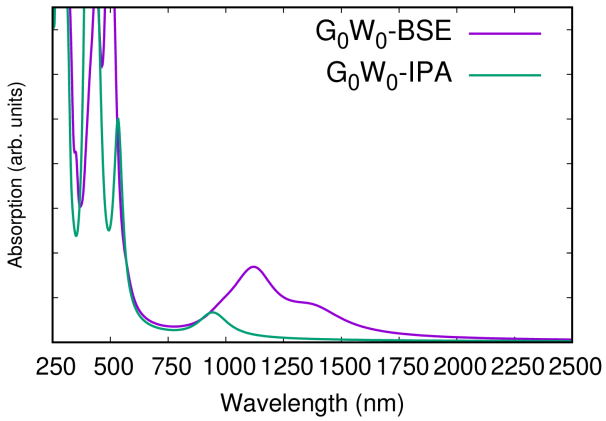

Figure S9: The relative dielectric function $\epsilon_r(\mathrm{E})$ is defined as $\epsilon_r(\mathrm{E}) = \epsilon_1(\mathrm{E}) + i\epsilon_2(\mathrm{E})$, where ϵ_1 and ϵ_2 are the real and imaginary parts of the dielectric function, respectively, and E is the photon energy (eV) related to wavelength λ (nm) through $\mathrm{E} = \frac{1239.8}{\lambda}$. In (a) and (b) we show the $\epsilon_1(\mathrm{E})$ and $\epsilon_2(\mathrm{E})$ as a function of photon energy for Co^{3+}-substituted t-YSZ configurations, respectively. The optical absorption spectrum is shown in (c). The color of the curve indicates different approximation level, where purple curve stands for G_0W_0-BSE and the green curve indicates the G_0W_0-IPA.

S1.10. Ni^{2+}

(a) Real part of the dielectric function (ϵ_1)

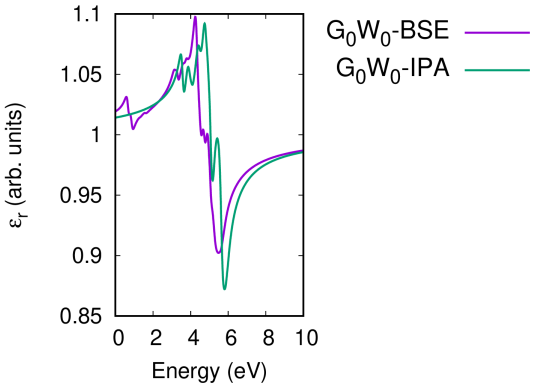

(b) Imaginary part of the dielectric function (ϵ_2)

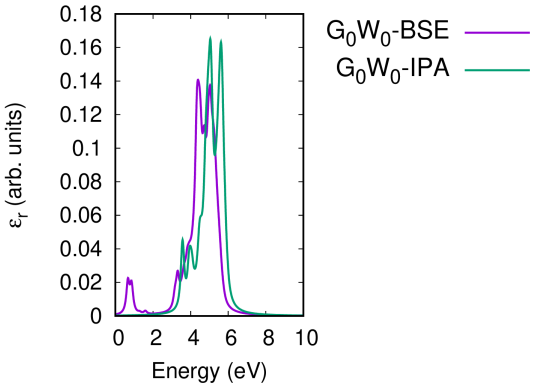

(c) Calculated optical absorption spectrum

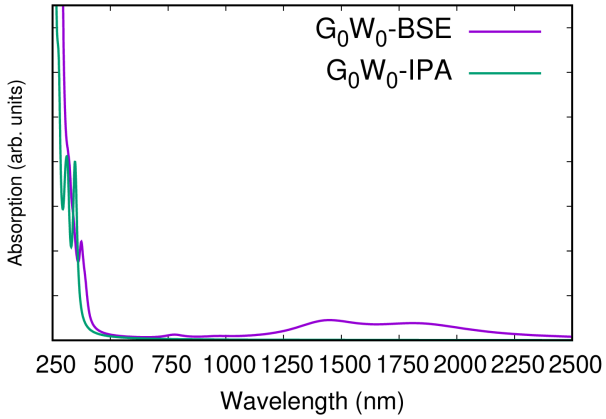

Figure S10: The relative dielectric function $\epsilon_r(\mathrm{E})$ is defined as $\epsilon_r(\mathrm{E}) = \epsilon_1(\mathrm{E}) + i\epsilon_2(\mathrm{E})$, where ϵ_1 and ϵ_2 are the real and imaginary parts of the dielectric function, respectively, and E is the photon energy (eV) related to wavelength λ (nm) through $\mathrm{E} = \frac{1239.8}{\lambda}$. In (a) and (b) we show the $\epsilon_1(\mathrm{E})$ and $\epsilon_2(\mathrm{E})$ as a function of photon energy for Ni^{2+}-substituted t-YSZ configurations, respectively. The optical absorption spectrum is shown in (c). The color of the curve indicates different approximation level, where purple curve stands for G_0W_0-BSE and the green curve indicates the G_0W_0-IPA.

S1.11. Ni^{3+}

(a) Real part of the dielectric function (ϵ_1)

(b) Imaginary part of the dielectric function (ϵ_2)

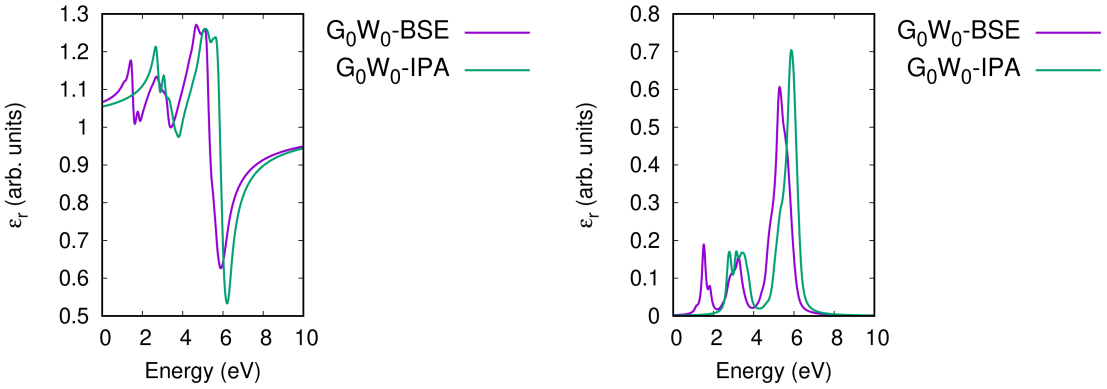

(c) Calculated optical absorption spectrum

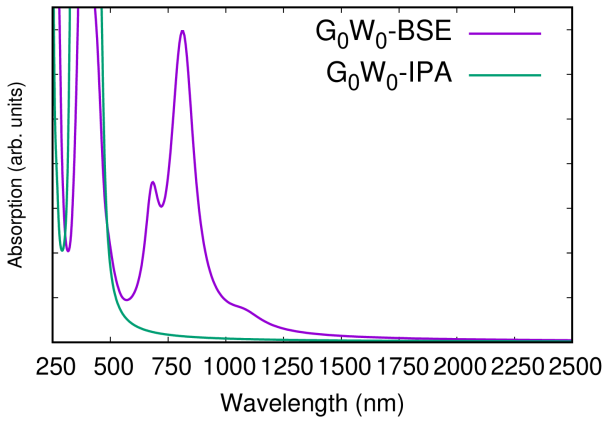

Figure S11: The relative dielectric function $\epsilon_r(\mathrm{E})$ is defined as $\epsilon_r(\mathrm{E}) = \epsilon_1(\mathrm{E}) + i\epsilon_2(\mathrm{E})$, where ϵ_1 and ϵ_2 are the real and imaginary parts of the dielectric function, respectively, and E is the photon energy (eV) related to wavelength λ (nm) through $\mathrm{E} = \frac{1239.8}{\lambda}$. In (a) and (b) we show the $\epsilon_1(\mathrm{E})$ and $\epsilon_2(\mathrm{E})$ as a function of photon energy for Ni^{3+}-substituted t-YSZ configurations, respectively. The optical absorption spectrum is shown in (c). The color of the curve indicates different approximation level, where purple curve stands for G_0W_0-BSE and the green curve indicates the G_0W_0-IPA.

S1.12. Cu^{2+}

(a) Real part of the dielectric function (ϵ_1)

(b) Imaginary part of the dielectric function (ϵ_2)

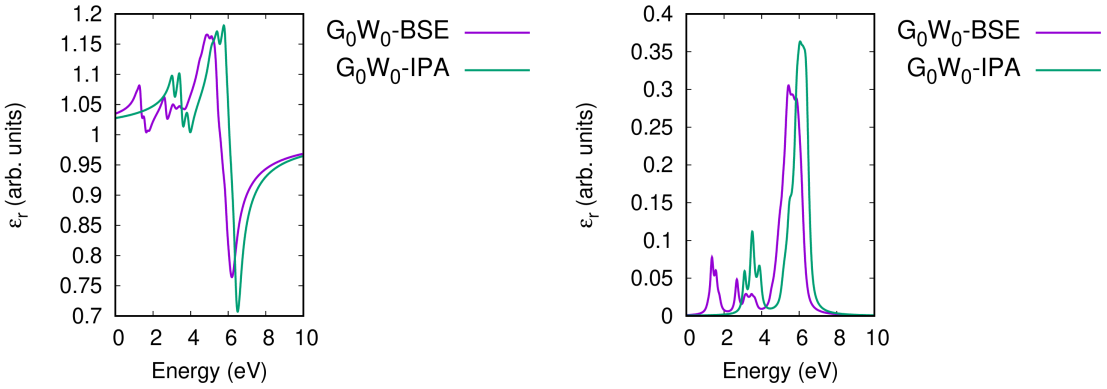

(c) Calculated optical absorption spectrum

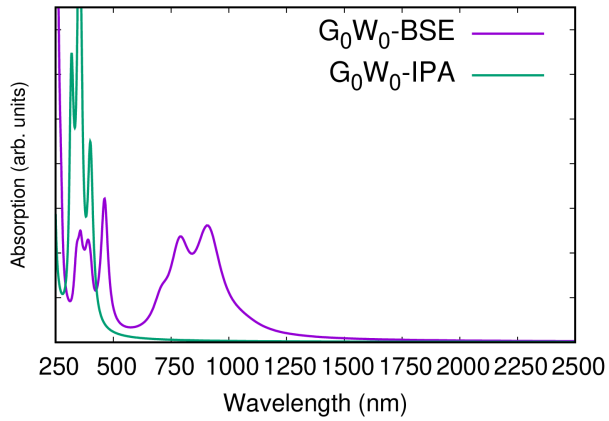

Figure S12: The relative dielectric function $\epsilon_r(\mathrm{E})$ is defined as $\epsilon_r(\mathrm{E}) = \epsilon_1(\mathrm{E}) + i\epsilon_2(\mathrm{E})$, where ϵ_1 and ϵ_2 are the real and imaginary parts of the dielectric function, respectively, and E is the photon energy (eV) related to wavelength λ (nm) through $\mathrm{E} = \frac{1239.8}{\lambda}$. In (a) and (b) we show the $\epsilon_1(\mathrm{E})$ and $\epsilon_2(\mathrm{E})$ as a function of photon energy for Cu^{2+}-substituted t-YSZ configurations, respectively. The optical absorption spectrum is shown in (c). The color of the curve indicates different approximation level, where purple curve stands for G_0W_0-BSE and the green curve indicates the G_0W_0-IPA.

S1.13. Zn^{2+}

(a) Real part of the dielectric function (ϵ_1)

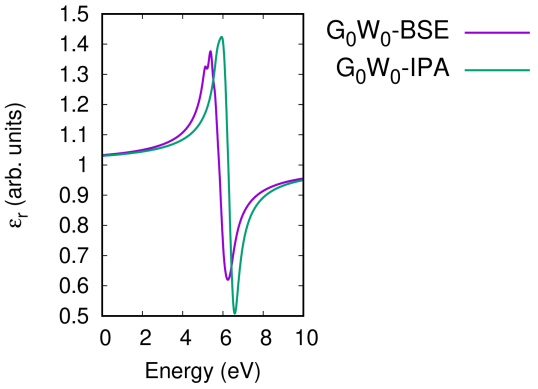

(b) Imaginary part of the dielectric function (ϵ_2)

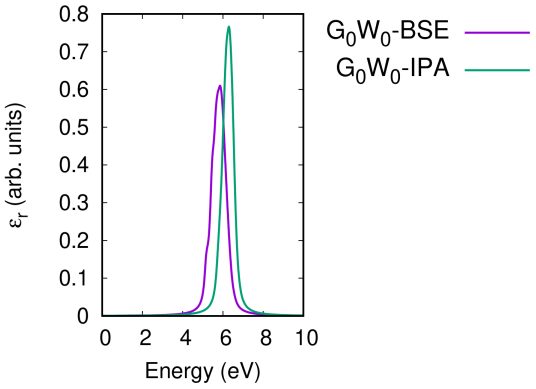

(c) Calculated optical absorption spectrum

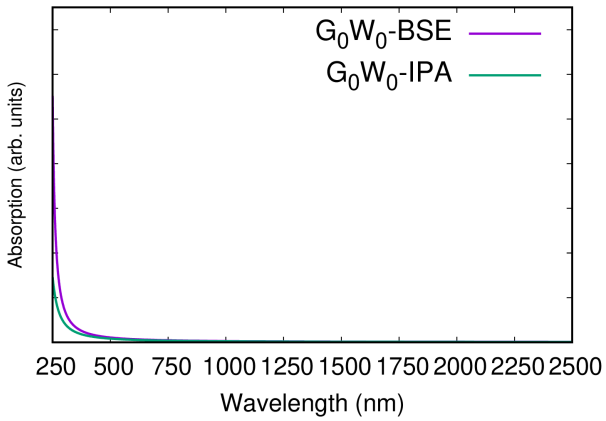

Figure S13: The relative dielectric function $\epsilon_r(\mathrm{E})$ is defined as $\epsilon_r(\mathrm{E}) = \epsilon_1(\mathrm{E}) + i\epsilon_2(\mathrm{E})$, where ϵ_1 and ϵ_2 are the real and imaginary parts of the dielectric function, respectively, and E is the photon energy (eV) related to wavelength λ (nm) through $\mathrm{E} = \frac{1239.8}{\lambda}$. In (a) and (b) we show the $\epsilon_1(\mathrm{E})$ and $\epsilon_2(\mathrm{E})$ as a function of photon energy for Zn^{2+}-substituted t-YSZ configurations, respectively. The optical absorption spectrum is shown in (c). The color of the curve indicates different approximation level, where purple curve stands for G_0W_0-BSE and the green curve indicates the G_0W_0-IPA.

S1.14. Ru^{3+}

(a) Real part of the dielectric function (ϵ_1)

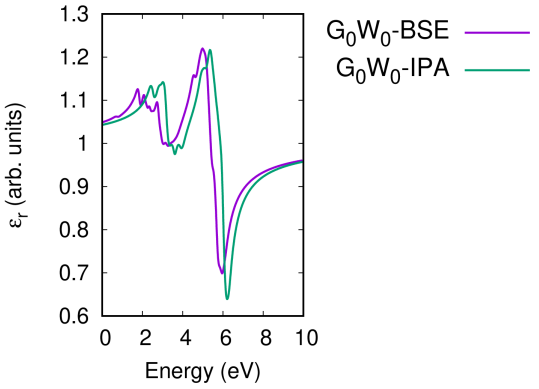

(b) Imaginary part of the dielectric function (ϵ_2)

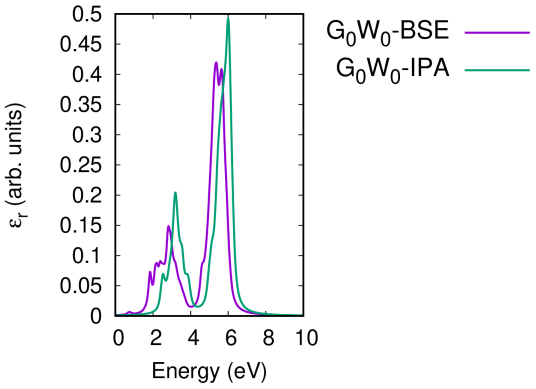

(c) Calculated optical absorption spectrum

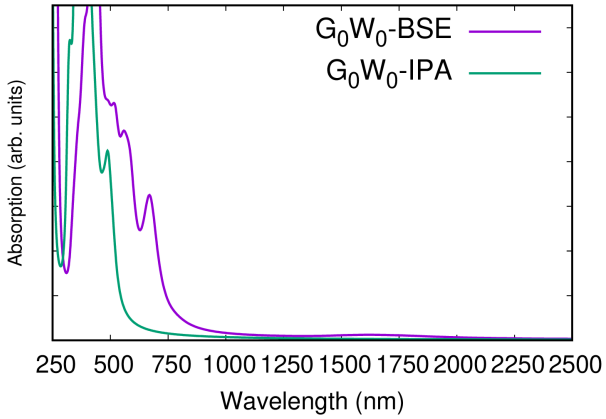

Figure S14: The relative dielectric function $\epsilon_r(\mathrm{E})$ is defined as $\epsilon_r(\mathrm{E}) = \epsilon_1(\mathrm{E}) + i\epsilon_2(\mathrm{E})$, where ϵ_1 and ϵ_2 are the real and imaginary parts of the dielectric function, respectively, and E is the photon energy (eV) related to wavelength λ (nm) through $\mathrm{E} = \frac{1239.8}{\lambda}$. In (a) and (b) we show the $\epsilon_1(\mathrm{E})$ and $\epsilon_2(\mathrm{E})$ as a function of photon energy for Ru^{3+}-substituted t-YSZ configurations, respectively. The optical absorption spectrum is shown in (c). The color of the curve indicates different approximation level, where purple curve stands for G_0W_0-BSE and the green curve indicates the G_0W_0-IPA.

S1.15. Ru^{4+}

(a) Real part of the dielectric function (ϵ_1)

(b) Imaginary part of the dielectric function (ϵ_2)

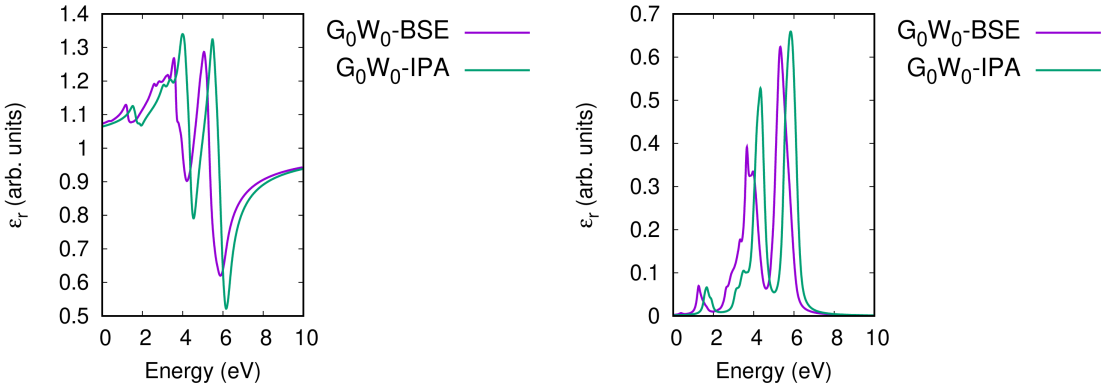

(c) Calculated optical absorption spectrum

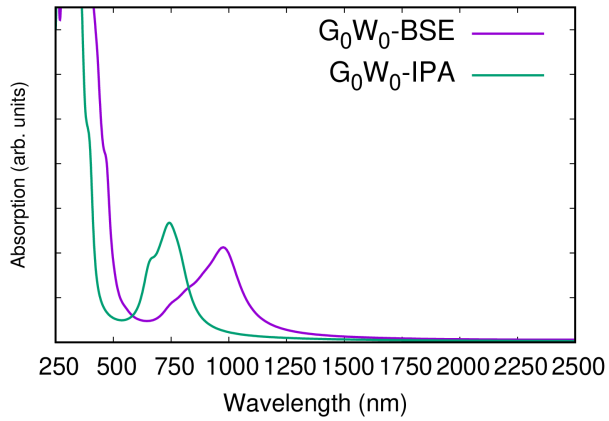

Figure S15: The relative dielectric function $\epsilon_r(\mathrm{E})$ is defined as $\epsilon_r(\mathrm{E}) = \epsilon_1(\mathrm{E}) + i\epsilon_2(\mathrm{E})$, where ϵ_1 and ϵ_2 are the real and imaginary parts of the dielectric function, respectively, and E is the photon energy (eV) related to wavelength λ (nm) through $\mathrm{E} = \frac{1239.8}{\lambda}$. In (a) and (b) we show the $\epsilon_1(\mathrm{E})$ and $\epsilon_2(\mathrm{E})$ as a function of photon energy for Ru^{4+}-substituted t-YSZ configurations, respectively. The optical absorption spectrum is shown in (c). The color of the curve indicates different approximation level, where purple curve stands for G_0W_0-BSE and the green curve indicates the G_0W_0-IPA.

S1.16. Os^{4+}

(a) Real part of the dielectric function (ϵ_1)

(b) Imaginary part of the dielectric function (ϵ_2)

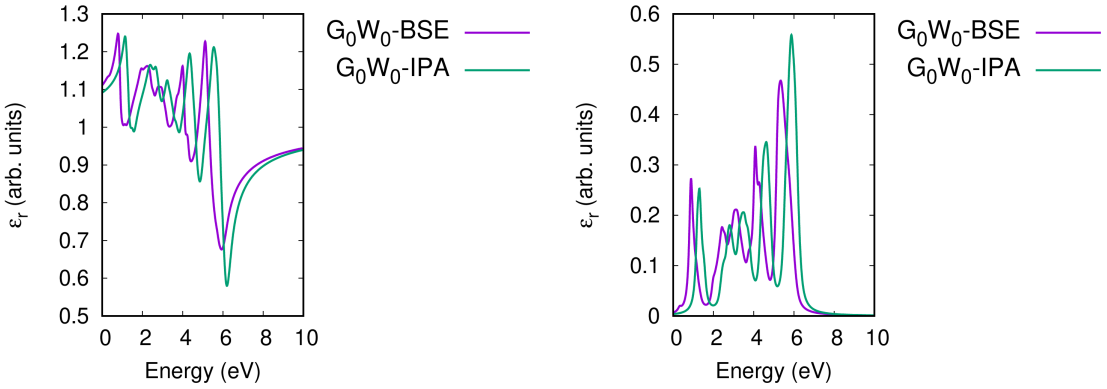

(c) Calculated optical absorption spectrum

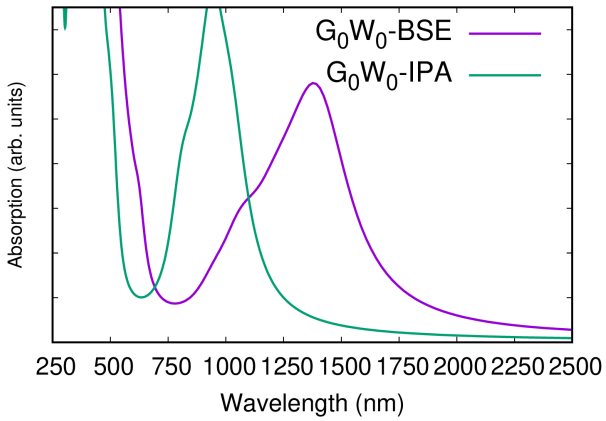

Figure S16: The relative dielectric function $\epsilon_r(\mathrm{E})$ is defined as $\epsilon_r(\mathrm{E}) = \epsilon_1(\mathrm{E}) + i\epsilon_2(\mathrm{E})$, where ϵ_1 and ϵ_2 are the real and imaginary parts of the dielectric function, respectively, and E is the photon energy (eV) related to wavelength λ (nm) through $\mathrm{E} = \frac{1239.8}{\lambda}$. In (a) and (b) we show the $\epsilon_1(\mathrm{E})$ and $\epsilon_2(\mathrm{E})$ as a function of photon energy for Os^{4+}-substituted t-YSZ configurations, respectively. The optical absorption spectrum is shown in (c). The color of the curve indicates different approximation level, where purple curve stands for G_0W_0-BSE and the green curve indicates the G_0W_0-IPA.

S2. PROJECTED DENSITY OF STATES AND EXCITON FOR EACH CONFIGURATION

S2.1. Ti^{4+}

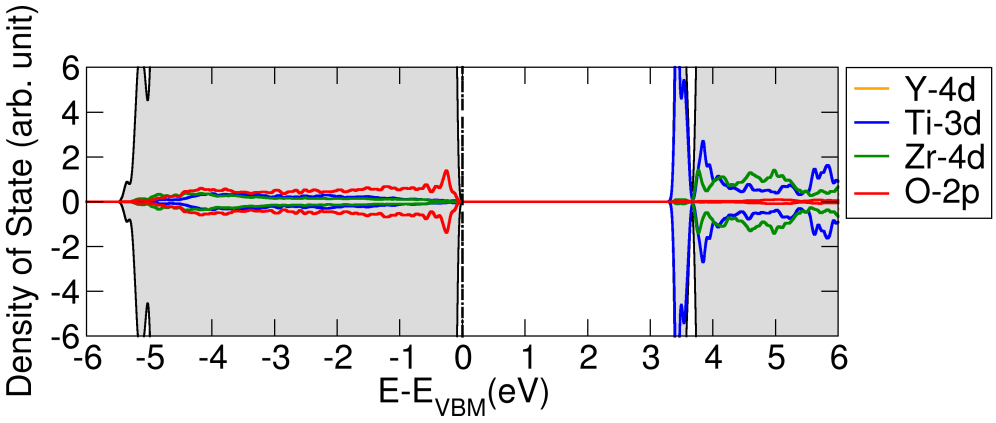

Figure S17: DFT projected density of states (PDOS) for Ti^{4+}-substituted tetragonal YSZ (t-YSZ). The energy is referenced to the valence band maximum (VBM), which is aligned at 0 eV. Positive and negative values correspond to the spin-up and spin-down channels, respectively. The gray background represents the total density of states, and the black dashed line indicates the position of the VBM.

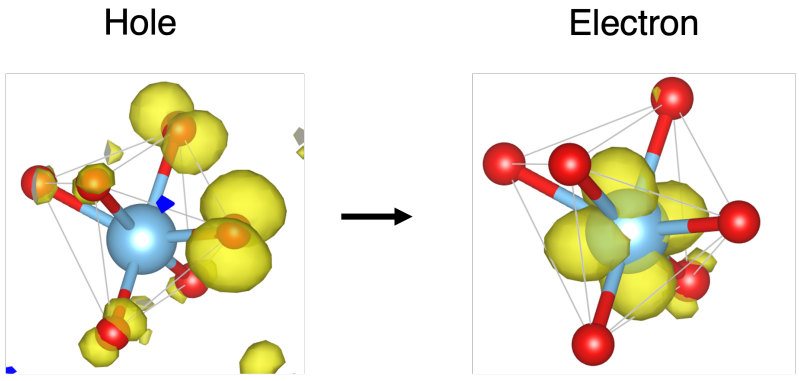

Figure S18: Hole and electron density distributions associated with the first exciton with a relative strength greater than 0.1 in Ti^{4+}-substituted t-YSZ. The corresponding excitation energy $E_{exc} = 4.36$ eV. The hole and electron density locate at different atoms inside the same polyhedron indicates a Type-I exciton, as discussed in Section III.

S2.2. V^{3+}

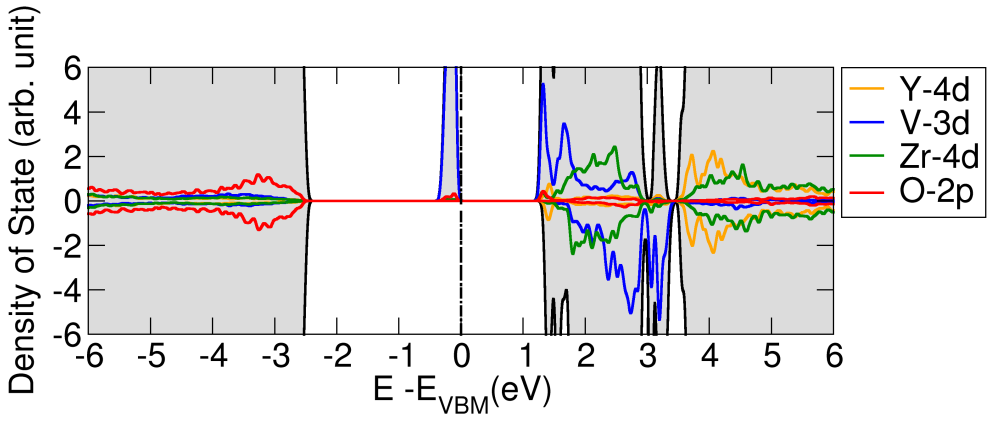

Figure S19: DFT projected density of states (PDOS) for V^{3+}-substituted tetragonal YSZ (t-YSZ). The energy is referenced to the valence band maximum (VBM), which is aligned at 0 eV. Positive and negative values correspond to the spin-up and spin-down channels, respectively. The gray background represents the total density of states, and the black dashed line indicates the position of the VBM.

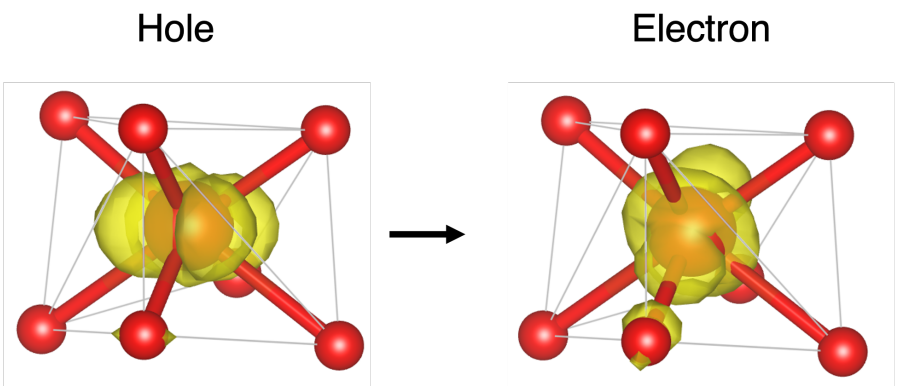

Figure S20: Hole and electron density distributions associated with the first exciton with a relative strength greater than 0.1 in V^{3+}-substituted t-YSZ. The corresponding excitation energy $E_{exc} = 1.09$ eV. The hole and electron density highly localized at V^{3+} cation indicates a Type-II exciton, as discussed in Section III.

S2.3. Cr^{3+}

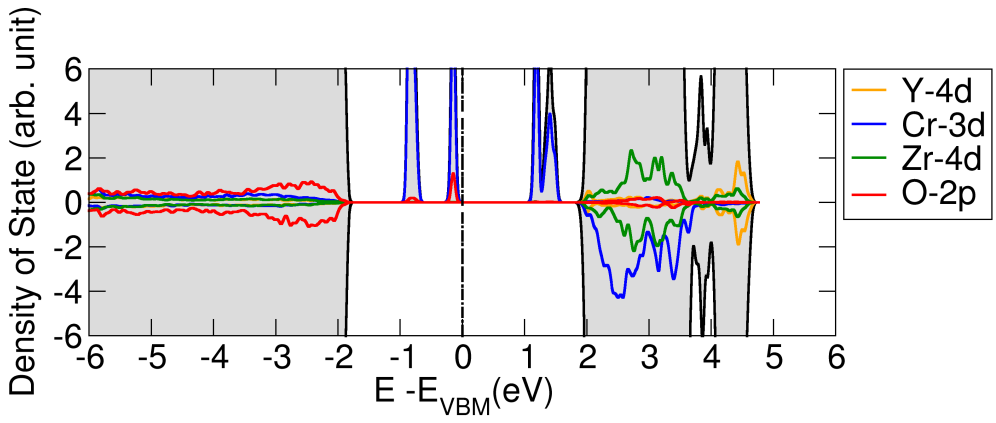

Figure S21: DFT projected density of states (PDOS) for Cr^{3+}-substituted tetragonal YSZ (t-YSZ). The energy is referenced to the valence band maximum (VBM), which is aligned at 0 eV. Positive and negative values correspond to the spin-up and spin-down channels, respectively. The gray background represents the total density of states, and the black dashed line indicates the position of the VBM.

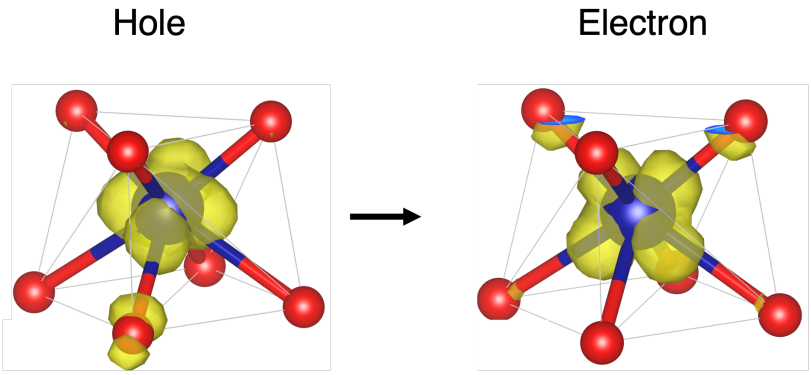

Figure S22: Hole and electron density distributions associated with the first exciton with a relative strength greater than 0.1 in Cr^{3+}-substituted t-YSZ. The corresponding excitation energy $E_{exc} = 0.99$ eV. The hole and electron density predominately localized at Cr^{3+} cation with a small fraction of hybridization with ligand O $2p$-orbital, indicating a Type-II exciton, as discussed in Section III.

S2.4. Cr^{6+}

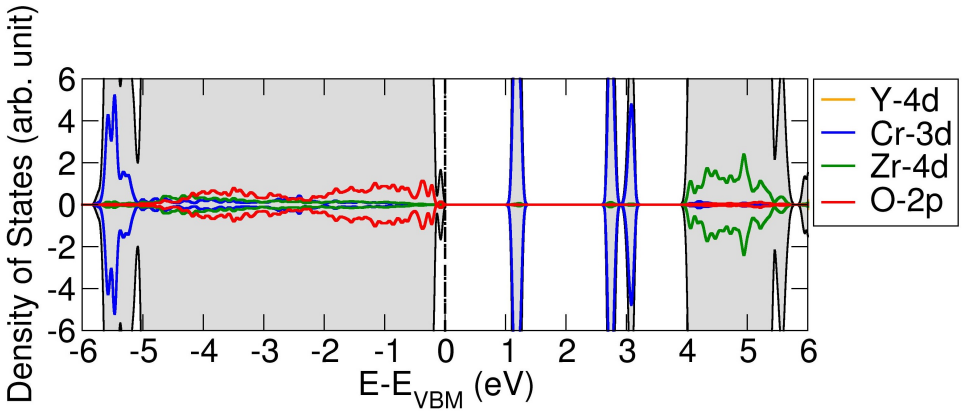

Figure S23: DFT projected density of states (PDOS) for Cr^{6+}-substituted tetragonal YSZ (t-YSZ). The energy is referenced to the valence band maximum (VBM), which is aligned at 0 eV. Positive and negative values correspond to the spin-up and spin-down channels, respectively. The gray background represents the total density of states, and the black dashed line indicates the position of the VBM.

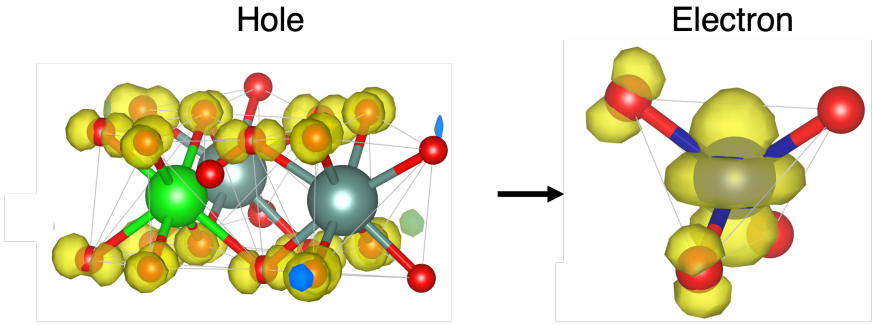

Figure S24: Hole and electron density distributions associated with the first exciton with a relative strength greater than 0.1 in Cr^{6+}-substituted t-YSZ. The corresponding excitation energy $E_{exc} = 2.76$ eV. The hole density located at multiple O $2p$-orbital across Zr and Y-centered polyhedron, while the electron density localized at Cr $3d$ and O $2p$-orbital within the Cr-centered polyhedron, indicating a Type-I′ exciton as discussed in Section III.

S2.5. Mn^{2+}

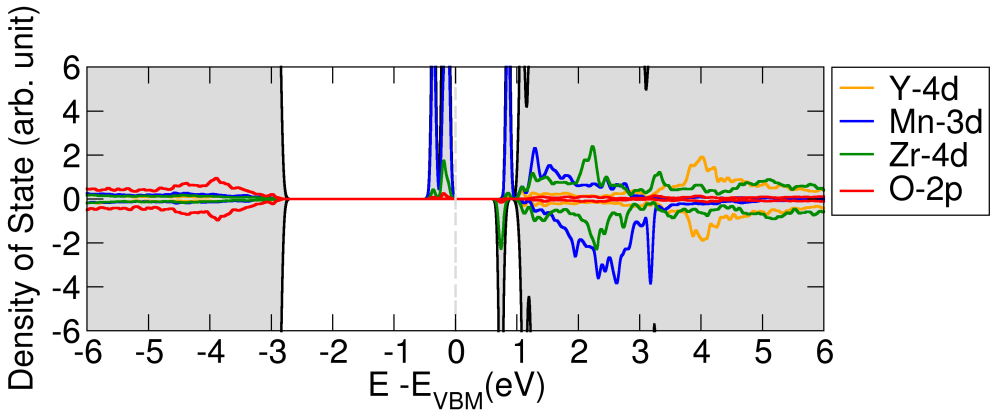

Figure S25: DFT projected density of states (PDOS) for Mn^{2+}-substituted tetragonal YSZ (t-YSZ). The energy is referenced to the valence band maximum (VBM), which is aligned at 0 eV. Positive and negative values correspond to the spin-up and spin-down channels, respectively. The gray background represents the total density of states, and the black dashed line indicates the position of the VBM.

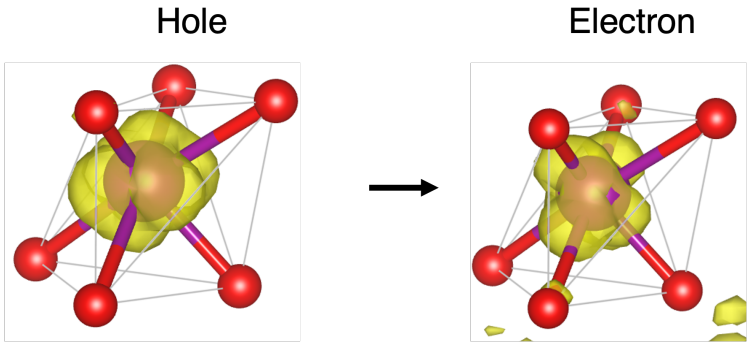

Figure S26: Hole and electron density distributions associated with the first exciton with a relative strength greater than 0.1 in Mn^{2+}-substituted t-YSZ. The corresponding excitation energy $E_{exc} = 1.91$ eV. The hole density is predominately localized at Mn^{2+} cation, and the electron density extended to Zr 4*d*-orbitals in other polyhedra. This character indicates a Type-II′ exciton as discussed in Section III.

S2.6. Mn^{3+}

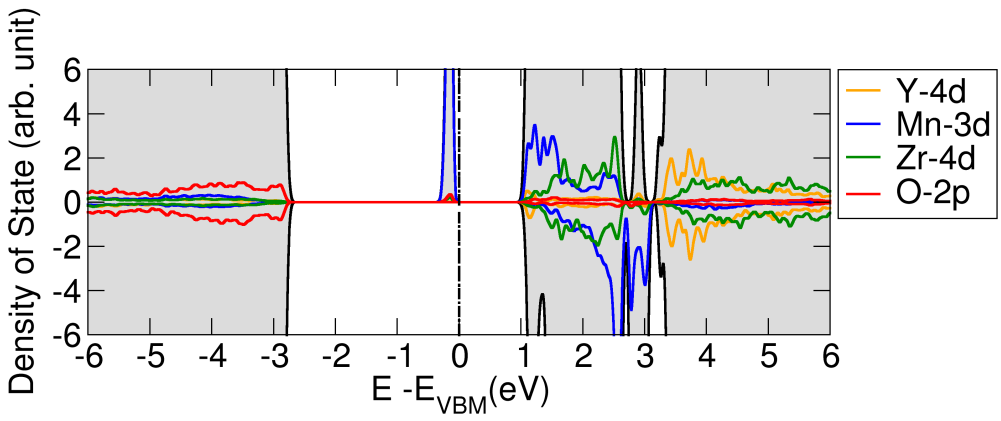

Figure S27: DFT projected density of states (PDOS) for Mn^{3+}-substituted tetragonal YSZ (t-YSZ). The energy is referenced to the valence band maximum (VBM), which is aligned at 0 eV. Positive and negative values correspond to the spin-up and spin-down channels, respectively. The gray background represents the total density of states, and the black dashed line indicates the position of the VBM.

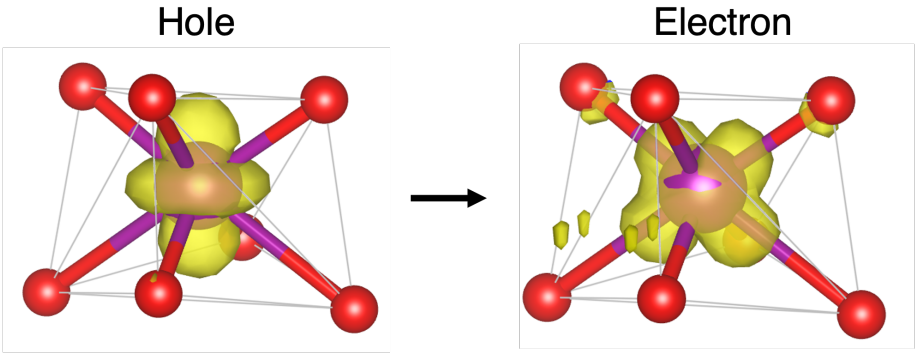

Figure S28: Hole and electron density distributions associated with the first exciton with a relative strength greater than 0.1 in Mn^{3+}-substituted t-YSZ. The corresponding excitation energy $E_{exc} = 1.31$ eV. The hole density is predominately localized at Mn^{2+} cation, and the electron density extended to ligand O $2p$-orbitals and Zr $4d$-orbitals in other polyhedra. This character indicates a Type-II′ exciton as discussed in Section III.

S2.7. Mn^{4+}

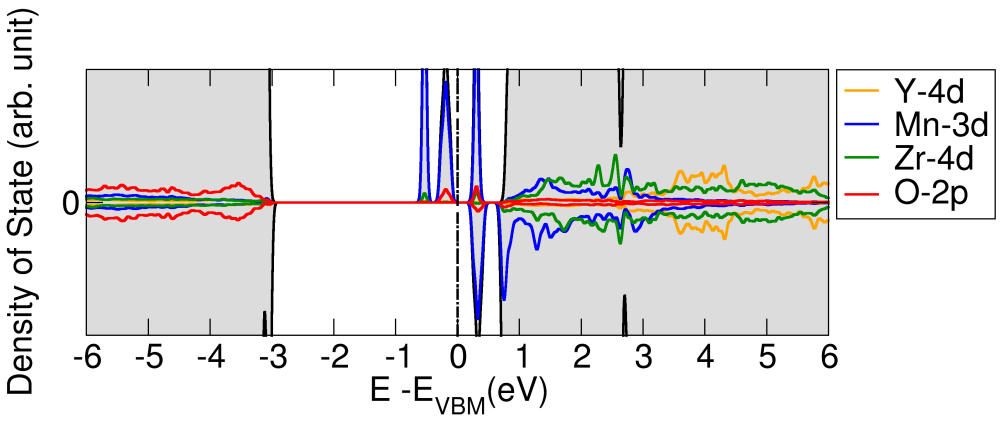

Figure S29: DFT projected density of states (PDOS) for Mn^{4+}-substituted tetragonal YSZ (t-YSZ). The energy is referenced to the valence band maximum (VBM), which is aligned at 0 eV. Positive and negative values correspond to the spin-up and spin-down channels, respectively. The gray background represents the total density of states, and the black dashed line indicates the position of the VBM.

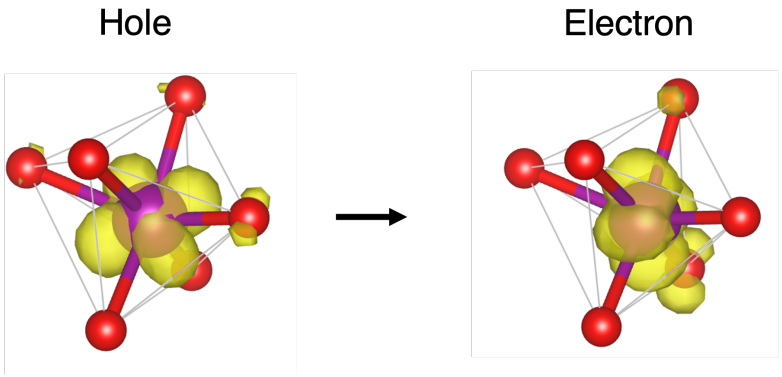

Figure S30: Hole and electron density distributions associated with the first exciton with a relative strength greater than 0.1 in Mn^{4+}-substituted t-YSZ. The corresponding excitation energy $E_{exc} = 1.81$ eV. The hole and electron density localized at Mn^{4+} cation with significant hybridization with ligand O $2p$-orbital, indicating a Type-II′ exciton, as discussed in Section III.

S2.8. Fe^{3+}

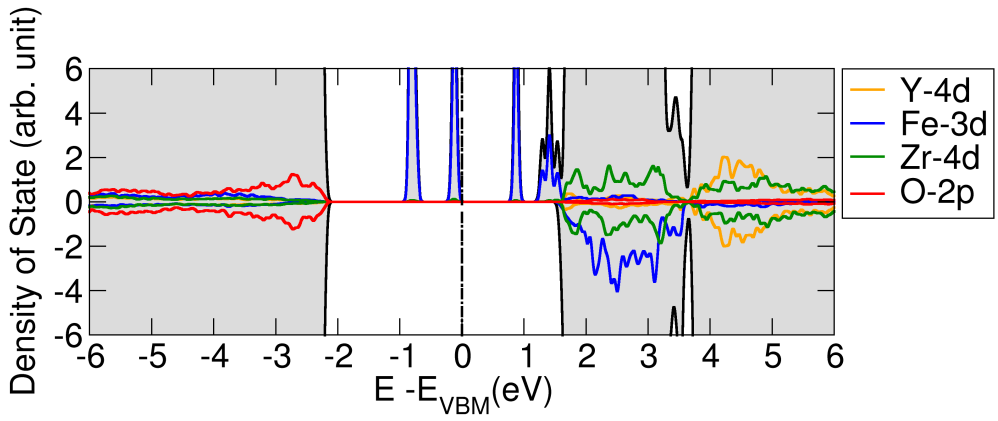

Figure S31: DFT projected density of states (PDOS) for Fe^{3+}-substituted tetragonal YSZ (t-YSZ). The energy is referenced to the valence band maximum (VBM), which is aligned at 0 eV. Positive and negative values correspond to the spin-up and spin-down channels, respectively. The gray background represents the total density of states, and the black dashed line indicates the position of the VBM.

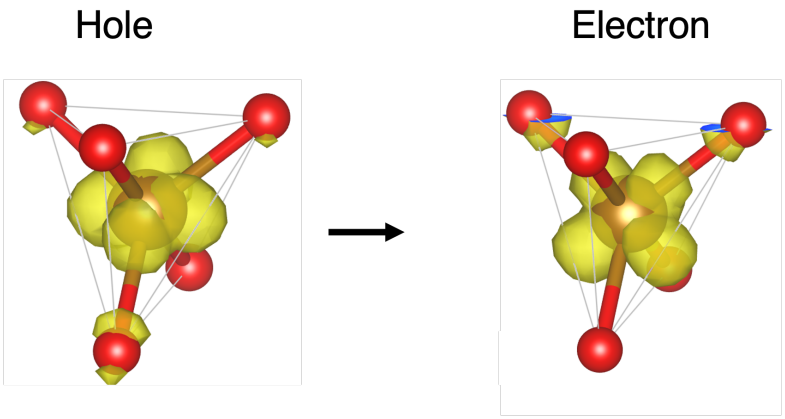

Figure S32: Hole and electron density distributions associated with the first exciton with a relative strength greater than 0.1 in Fe^{3+}-substituted t-YSZ. The corresponding excitation energy $E_{exc} = 0.70$ eV. The hole and electron density highly localized at Fe^{3+} cation indicates a Type-II exciton, as discussed in Section III.

S2.9. Co^{3+}

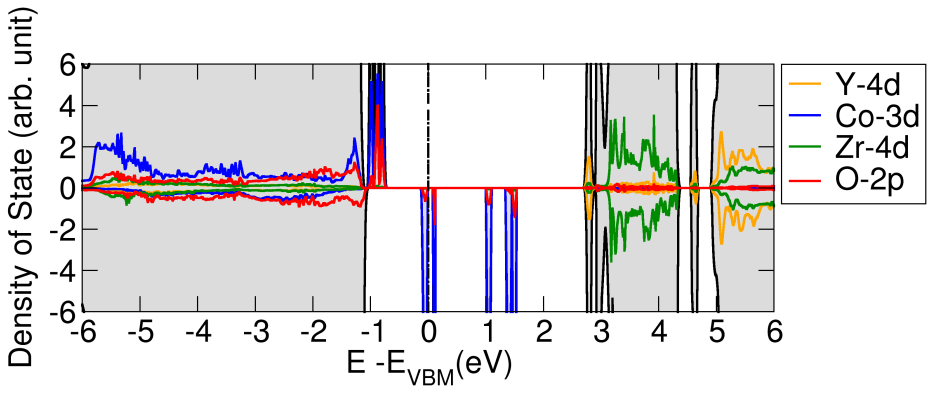

Figure S33: DFT projected density of states (PDOS) for Co^{3+}-substituted tetragonal YSZ (t-YSZ). The energy is referenced to the valence band maximum (VBM), which is aligned at 0 eV. Positive and negative values correspond to the spin-up and spin-down channels, respectively. The gray background represents the total density of states, and the black dashed line indicates the position of the VBM. For this specific PDOS, we did not add any gaussian smearing due the narrow gap.

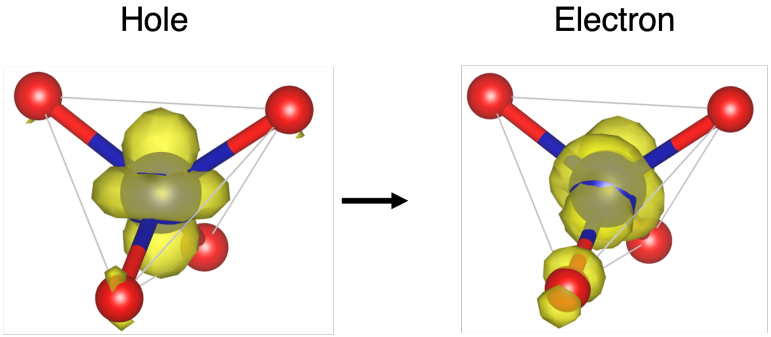

Figure S34: Hole and electron density distributions associated with the first exciton with a relative strength greater than 0.1 in Co^{3+}-substituted t-YSZ. The corresponding excitation energy $E_{exc} = 0.89$ eV. The hole and electron density highly localized at Co^{3+} cation with hybridization with O 2*p*-orbital, indicating a Type-II′ exciton, as discussed in Section III.

S2.10. Ni^{2+}

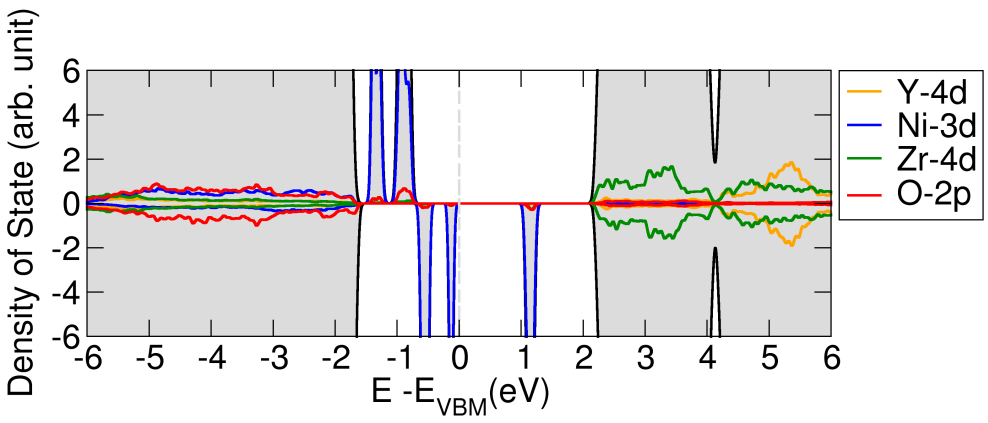

Figure S35: DFT projected density of states (PDOS) for Ni^{2+}-substituted tetragonal YSZ (t-YSZ). The energy is referenced to the valence band maximum (VBM), which is aligned at 0 eV. Positive and negative values correspond to the spin-up and spin-down channels, respectively. The gray background represents the total density of states, and the black dashed line indicates the position of the VBM.

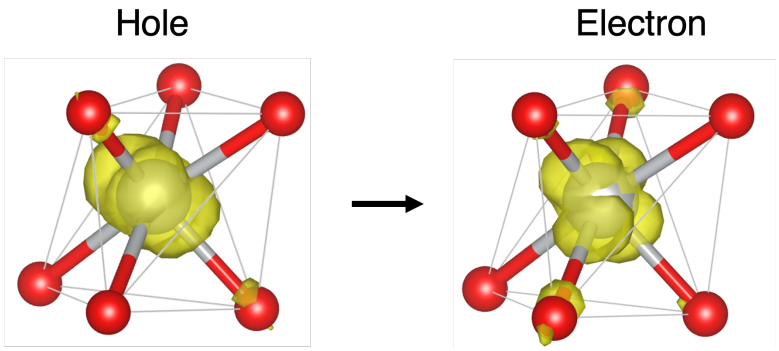

Figure S36: Hole and electron density distributions associated with the first exciton with a relative strength greater than 0.1 in Ni^{2+}-substituted t-YSZ. The corresponding excitation energy $E_{exc} = 0.57$ eV. The hole and electron density highly localized at Ni^{2+} cation, indicating a Type-II exciton, as discussed in Section III.

S2.11. Ni^{3+}

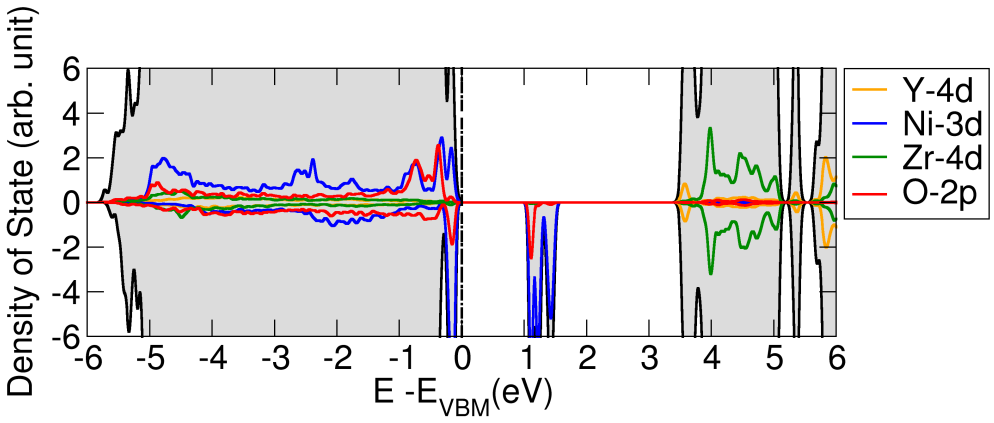

Figure S37: DFT projected density of states (PDOS) for Ni^{3+}-substituted tetragonal YSZ (t-YSZ). The energy is referenced to the valence band maximum (VBM), which is aligned at 0 eV. Positive and negative values correspond to the spin-up and spin-down channels, respectively. The gray background represents the total density of states, and the black dashed line indicates the position of the VBM.

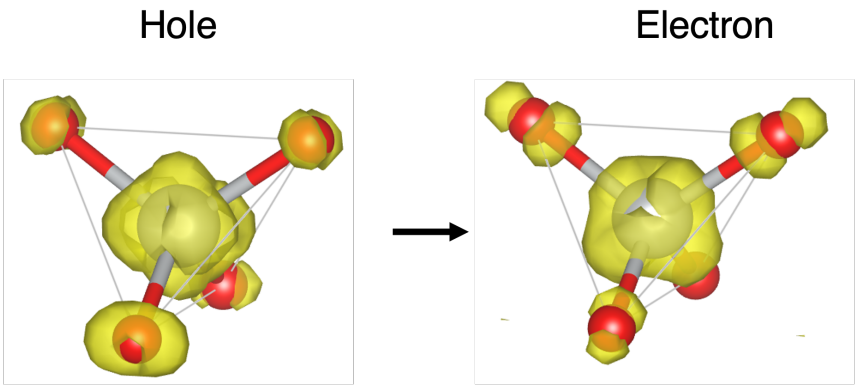

Figure S38: Hole and electron density distributions associated with the first exciton with a relative strength greater than 0.1 in Ni^{3+}-substituted t-YSZ. The corresponding excitation energy $E_{exc} = 1.50$ eV. The hole and electron density localized at Ni^{3+} cation with significant hybridization with ligand O $2p$-orbital, indicating a Type-II′ exciton, as discussed in Section III.

S2.12. Cu^{2+}

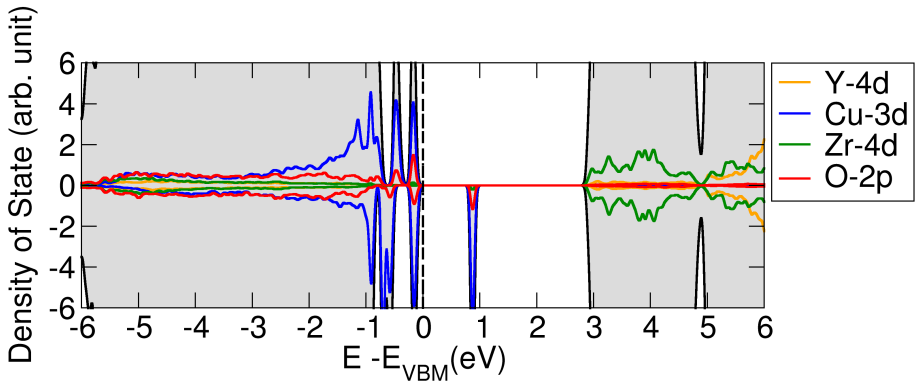

Figure S39: DFT projected density of states (PDOS) for Cu^{2+}-substituted tetragonal YSZ (t-YSZ). The energy is referenced to the valence band maximum (VBM), which is aligned at 0 eV. Positive and negative values correspond to the spin-up and spin-down channels, respectively. The gray background represents the total density of states, and the black dashed line indicates the position of the VBM.

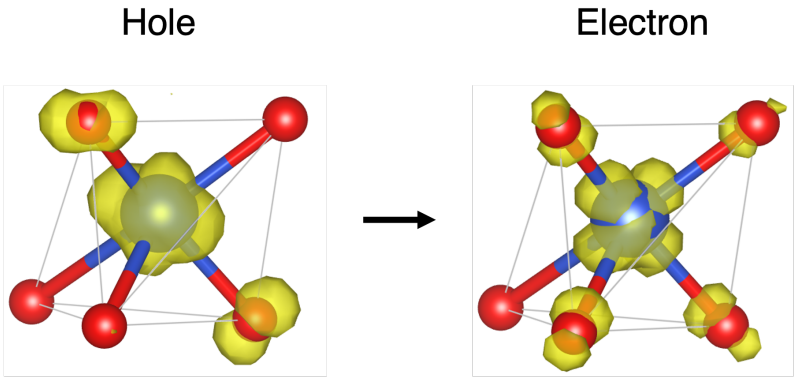

Figure S40: Hole and electron density distributions associated with the first exciton with a relative strength greater than 0.1 in Cu^{2+}-substituted t-YSZ. The corresponding excitation energy $E_{exc} = 1.66$ eV. The hole and electron density localized at Cu^{2+} cation with significant hybridization with ligand O $2p$-orbital, indicating a Type-II′ exciton, as discussed in Section III.

S2.13. Zn^{2+}

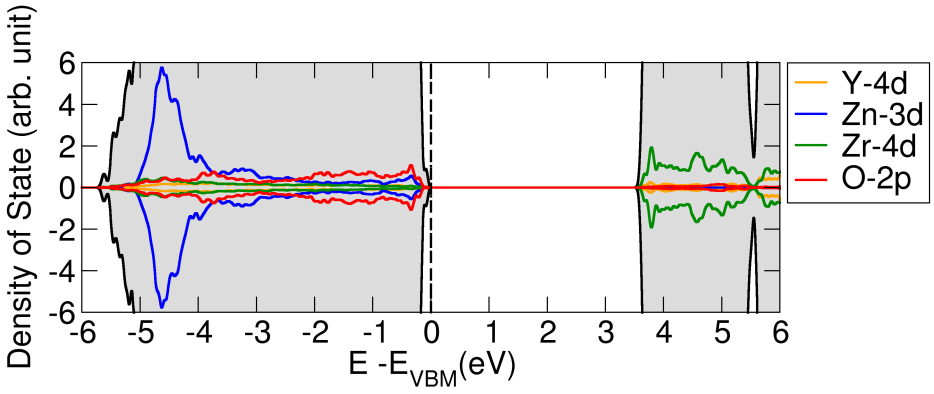

Figure S41: DFT projected density of states (PDOS) for Zn^{2+}-substituted tetragonal YSZ (t-YSZ). The energy is referenced to the valence band maximum (VBM), which is aligned at 0 eV. Positive and negative values correspond to the spin-up and spin-down channels, respectively. The gray background represents the total density of states, and the black dashed line indicates the position of the VBM.

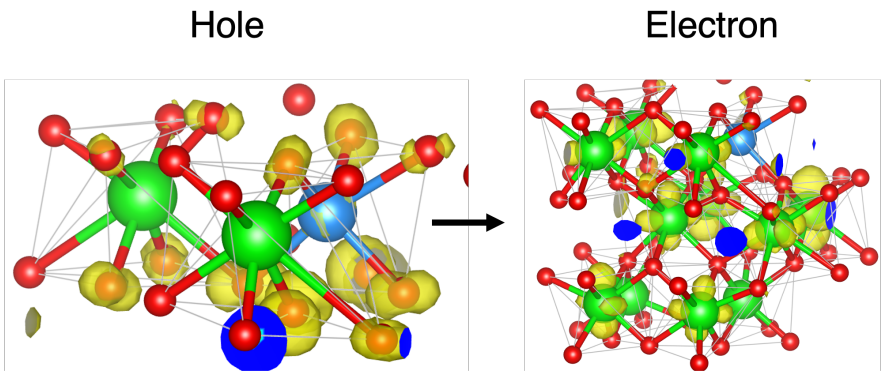

Figure S42: Hole and electron density distributions associated with the first exciton with a relative strength greater than 0.1 in Zn^{2+}-substituted t-YSZ. The corresponding excitation energy $E_{exc} = 0.52$ eV. The hole and electron density locate at different atoms inside Zr-centered polyhedron indicates a Type-I exciton, as discussed in Section III.

S2.14. Ru^{3+}

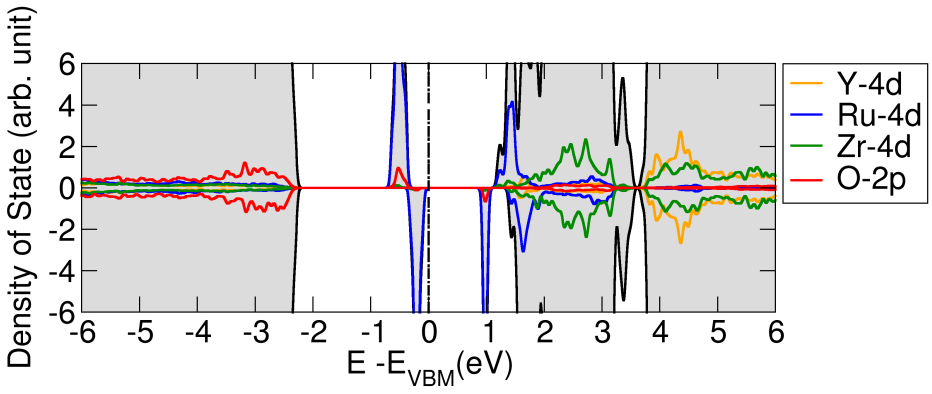

Figure S43: DFT projected density of states (PDOS) for Ru^{3+}-substituted tetragonal YSZ (t-YSZ). The energy is referenced to the valence band maximum (VBM), which is aligned at 0 eV. Positive and negative values correspond to the spin-up and spin-down channels, respectively. The gray background represents the total density of states, and the black dashed line indicates the position of the VBM.

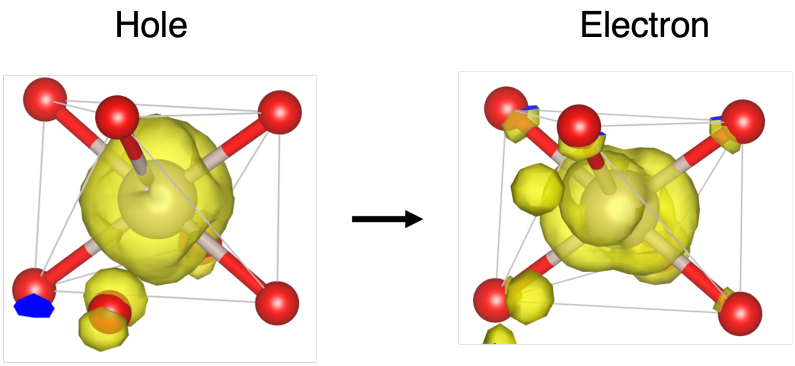

Figure S44: Hole and electron density distributions associated with the first exciton with a relative strength greater than 0.1 in Ru^{3+}-substituted t-YSZ. The corresponding excitation energy $E_{exc} = 1.84$ eV. The hole and electron density localized at Ru^{3+} cation with significant hybridization with ligand O $2p$-orbital, indicating a Type-II′ exciton, as discussed in Section III.

S2.15. Ru^{4+}

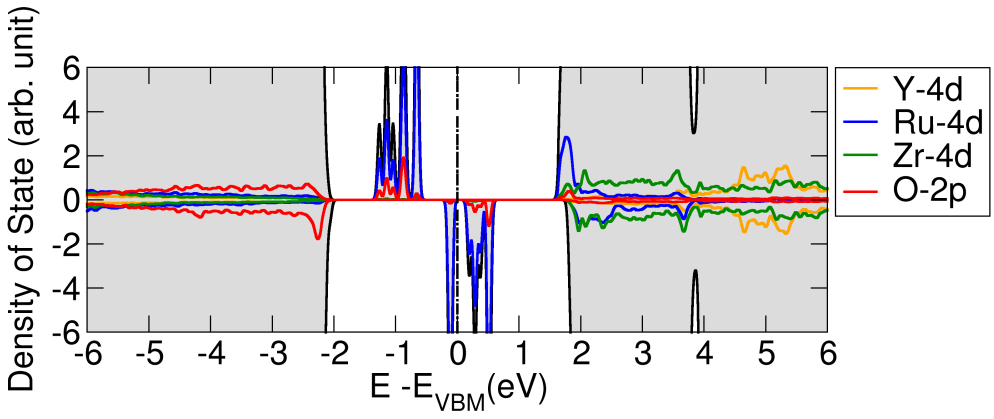

Figure S45: DFT projected density of states (PDOS) for Ru^{4+}-substituted tetragonal YSZ (t-YSZ). The energy is referenced to the valence band maximum (VBM), which is aligned at 0 eV. Positive and negative values correspond to the spin-up and spin-down channels, respectively. The gray background represents the total density of states, and the black dashed line indicates the position of the VBM.

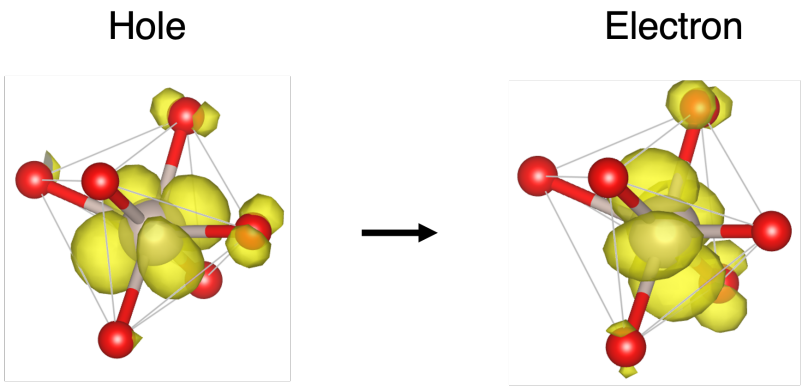

Figure S46: Hole and electron density distributions associated with the first exciton with a relative strength greater than 0.1 in Ru^{4+}-substituted t-YSZ. The corresponding excitation energy $E_{exc} = 1.26$ eV. The hole and electron density highly localized at Ru^{4+} cation with significant hybridization with ligand O $2p$-orbital, indicating a Type-II′ exciton, as discussed in Section III.

S2.16. Os^{4+}

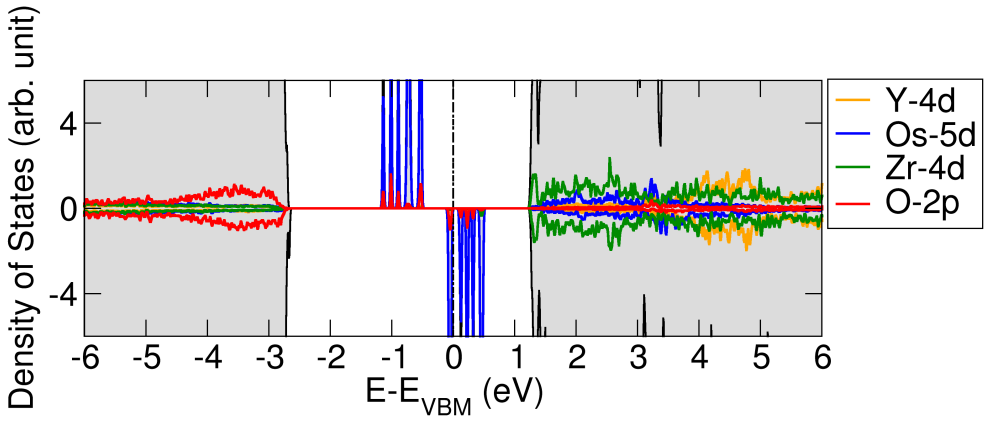

Figure S47: DFT projected density of states (PDOS) for Os^{4+}-substituted tetragonal YSZ (t-YSZ). The energy is referenced to the valence band maximum (VBM), which is aligned at 0 eV. Positive and negative values correspond to the spin-up and spin-down channels, respectively. The gray background represents the total density of states, and the black dashed line indicates the position of the VBM.

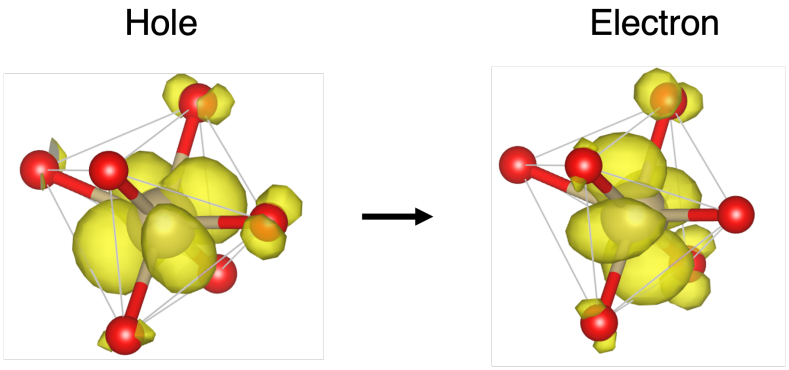

Figure S48: Hole and electron density distributions associated with the first exciton with a relative strength greater than 0.1 in Os^{4+}-substituted t-YSZ. The corresponding excitation energy $E_{exc} = 0.86$ eV. The hole and electron density highly localized at Os^{4+} cation with significant hybridization with ligand O $2p$-orbital, indicating a Type-II′ exciton, as discussed in Section III.